Insertion of c-*Myc* into *Igh* Induces B-Cell and Plasma-Cell Neoplasms in Mice

Sung Sup Park,[1] Joong Su Kim,[1] Lino Tessarollo,[4] James D. Owens,[1] Liangping Peng,[1] Seong Su Han,[1] Seung Tae Chung,[1] Ted A. Torrey,[3] Wan C. Cheung,[5] Roberto D. Polakiewicz,[6] Nicole McNeil,[2] Thomas Ried,[2] J. Frederic Mushinski,[1] Herbert C. Morse III,[3] and Siegfried Janz[1]

[1]Laboratory of Genetics, [2]Genetics Branch, Center for Cancer Research, National Cancer Institute, and [3]Laboratory of Immunopathology, National Institute of Allergy and Infectious Diseases, NIH, Bethesda, Maryland; [4]Laboratory for Neural Development, Center for Cancer Research, National Cancer Institute, Frederick, Maryland; and [5]Cell Signaling Technology, Beverly, Massachusetts

Abstract

We used gene targeting in mice to insert a His_6-tagged mouse c-*Myc* cDNA, Myc^{His}, head to head into the mouse immunoglobulin heavy-chain locus, *Igh*, just 5′ of the intronic enhancer, Eμ. The insertion of Myc^{His} mimicked both the human t(8;14)(q24;q32) translocation that results in the activation of *MYC* in human endemic Burkitt lymphomas and the homologous mouse T(12;15) translocation that deregulates *Myc* in certain mouse plasmacytomas. Beginning at the age of 6 months, Myc^{His} transgenic mice developed B-cell and plasma neoplasms, such as IgM^+ lymphoblastic B-cell lymphomas, Bcl-6^+ diffuse large B-cell lymphomas, and $CD138^+$ plasmacytomas, with an overall incidence of 68% by 21 months. Molecular studies of lymphoblastic B-cell lymphoma, the most prevalent neoplasm (50% of all tumors), showed that the lymphomas were clonal, overexpressed Myc^{His}, and exhibited the P2 to P1 promoter shift in *Myc* expression, a hallmark of *MYC/Myc* deregulation in human endemic Burkitt lymphoma and mouse plasmacytoma. Only 1 (6.3%) of 16 lymphoblastic B-cell lymphomas contained a BL-typical point mutation in the amino-terminal transactivation domain of Myc^{His}, suggesting that most of these tumors are derived from naive, pregerminal center B cells. Twelve (46%) of 26 lymphoblastic B-cell lymphomas exhibited changes in the $p19^{Arf}$-Mdm2-p53 tumor suppressor axis, an important pathway for Myc-dependent apoptosis. We conclude that Myc^{His} insertion into *Igh* predictably induces B-cell and plasma-cell tumors in mice, providing a valuable mouse model for understanding the transformation-inducing consequences of the *MYC/Myc*-activating endemic Burkitt lymphoma t(8;14)/plasmacytoma T(12;15) translocation. (Cancer Res 2005; 65(4): 1306–15)

Introduction

Reciprocal chromosomal translocations that activate the cellular oncogene *MYC* are widely accepted as the initiating events in the natural history of human endemic Burkitt lymphoma, an aggressive form of mature, postgerminal center, non-Hodgkin lymphoma. The most common translocation found in endemic Burkitt lymphoma is t(8;14)(q24;q32), which recombines *MYC* at 8q24 with the immunoglobulin heavy-chain gene locus, *IGH*, at 14q32 (1, 2). The breakpoints of t(8;14) usually occur in the joining gene region of the *IGH* locus, J_H, and in the 5′ flank of *MYC*. The resulting exchanges allocate the intact *MYC* gene, including the noncoding regulatory first exon with the two major *MYC* promoters, P1 and P2, to the *MYC*-deregulated product of translocation, where *MYC* is apposed to the intronic heavy-chain enhancer, Eμ, in opposite transcriptional orientation (Fig. 1). Mouse plasmacytoma, a malignant tumor of terminally differentiated B cells, is thought to be initiated, just like human endemic Burkitt lymphoma, by *Myc*-activating chromosomal translocations (3). The most common translocation observed in plasmacytoma is the T(12;15), the direct counterpart of the human t(8;14) translocation. A recent molecular analysis of T(12;15) in IL-6 transgenic plasmacytomas and their precursors has shown that 8 (18%) of 45 translocation breakpoint regions exhibited the endemic Burkitt lymphoma t(8;14)-typical *Myc*-Eμ juxtaposition on the *Myc*-deregulated product of translocation (Fig. 1; ref. 4). Thus, homologous *MYC/Myc*-Eμ rearrangements lead to B-cell and plasma-cell neoplasms in humans and mice.

The mechanism by which human endemic Burkitt lymphoma t(8;14) and mouse plasmacytoma T(12;15) deregulate the expression of *MYC/Myc* and, thereby, promote the malignant transformation of B lymphocytes and plasma cells has not been shown (5). Further insights into this mechanism might be possible if a mouse model that accurately reproduces the key features of the endemic Burkitt lymphoma t(8;14)/plasmacytoma T(12;15) could be produced. Previous attempts to develop such a model used mice that harbor multiple copies of human *MYC* or mouse *Myc* under control of the human or mouse Eμ enhancer (6–9). Clearly, the Eμ-driven *MYC/Myc* genes are incomplete models of the endemic Burkitt lymphoma t(8;14)/plasmacytoma T(12;15) because they reproduce just one aspect of this translocation, the juxtaposition of Eμ and *MYC/Myc* (5). Another approach used mice that carry a 240-kb single-copy yeast artificial chromosome (YAC), which consists of a human germ line VDJ-Cμ-Cδ locus and the *MYC* gene from the BL cell line Raji (10, 11). Serious shortcomings of the YAC-MYC approach include the absence of the Eα enhancer, which is believed to be the critical element for *MYC* up-regulation in tumors of late B and plasma cells (12), the unusual location of *MYC* in the *IGH* locus (3′ of Cδ) and the head-to-tail orientation of *MYC* relative to *IGH*, features that are not observed in human endemic Burkitt lymphoma or mouse plasmacytoma. Consistent with the apparent inability of the YAC-MYC and Eμ-MYC/Myc transgenes to faithfully recreate the endemic Burkitt lymphoma t(8;14)/plasmacytoma T(12;15), the transgenic mice develop predominantly lymphomas with features of pre-B, immature B, or transitional B cells, rather than mature B cells

Note: S.S. Park, J.S. Kim, and L. Tessarollo contributed equally to this article and are thus sharing first authorship. S.S. Park and J.S. Kim are currently in Laboratory of Functional Proteomics, Korea Research Institute of Bioscience and Biotechnology, Taejon, Korea.

Supplementary data for this article are available at Cancer Research Online (http://cancerres.aacrjournals.org/).

Requests for reprints: Siegfried Janz, Laboratory of Genetics, Center for Cancer Research, National Cancer Institute, Building 37, Room 3140A, Bethesda, MD 20892-4256. Phone: 301-496-2202; Fax: 301-402-1031; E-mail: sj4s@nih.gov.

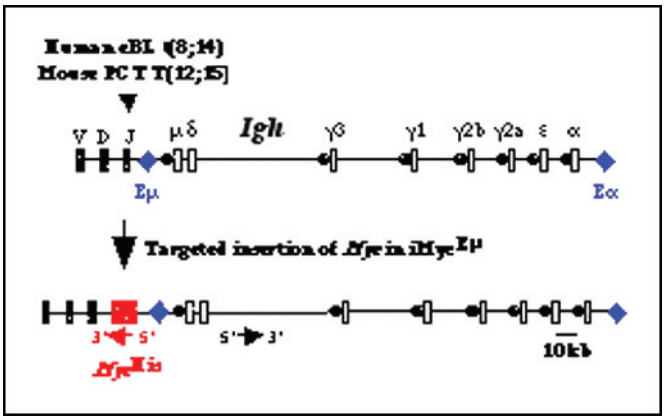

Figure 1. Targeted transgenic insertion of Myc^{His} in $iMyc^{E\mu}$ mice. Shown is a scheme of the normal mouse *Igh* locus (*top*) and the targeted *Igh* locus (*bottom*) with the inserted Myc^{His} in $iMyc^{E\mu}$ mice (*red*). The Eμ and Eα enhancers are depicted by *blue diamonds*. The transcriptional orientations of *Igh* and *Myc* are indicated by *black and red arrows*, respectively. The gene insertion site is also the preferred recombination site of human t(8;14)(q24;q32) *IGH-MYC* exchanges in human endemic Burkitt lymphoma and mouse T(12;15) *Igh-Myc* exchanges in certain mouse plasmacytomas.

(human endemic Burkitt lymphoma) or plasma cells (mouse plasmacytoma).

To model endemic Burkitt lymphoma t(8;14)/plasmacytoma T(12;15) more precisely, we inserted a His_6-tagged mouse *Myc* cDNA in the J_H-Eμ intervening region of mouse *Igh* and developed a mouse strain, designated $iMyc^{E\mu}$, in which *Myc* is juxtaposed head to head with Eμ, just as in human endemic Burkitt lymphoma and mouse plasmacytoma (Fig. 1). Between the age of 6 and 21 months, nearly 70% of the heterozygous $iMyc^{E\mu}$ mice developed lymphoblastic B-cell lymphomas with a BL-like morphology, diffuse large B-cell lymphomas and plasmacytomas. All these are tumors of mature B cells. The observed spectrum of tumors provided strong empirical evidence that the $iMyc^{E\mu}$ transgene mimicked the critical features of the endemic Burkitt lymphoma t(8;14)/plasmacytoma T(12;15) translocation.

Materials and Methods

Generation of $iMyc^{E\mu}$ Mice. Gene targeting (13) and cre-loxP recombination (14) were used to insert a mouse *Myc* gene into the mouse germ line *Igh* locus. The inserted *Myc* consisted of an intronless cDNA clone, the noncoding first exon with the natural P1/P2 promoter, 1.5 kb of genomic 5′ flank containing the normal transcription-regulatory region, and a short stretch of 3′ untranslated region harboring the *Myc* major polyadenylation site. The untranslated region downstream of the polyadenylate signal, which has been shown to be dispensable *in vivo* (15), was not present in the construct. The *Myc* also contained the coding sequence for an artificial histidine tag, His_6, added in frame at the 3′ end of the gene. The tag made it possible to distinguish *Myc* mRNA and Myc protein encoded by the inserted Myc^{His} gene on chromosome 12 from the endogenous *Myc* gene (no tag) on chromosome 15. Myc^{His} was inserted in the intervening region between J_H4 and Eμ, ~0.5 kb 5′ of Eμ, in opposite transcriptional orientation to *Igh*. The construction of the inserted gene, $Myc^{His}Neo^{loxP}$, the assembly of the targeting vector, and the generation of *Neo*-less $iMyc^{E\mu}$ mice are described in the Supplementary Materials and Methods section and illustrated in Supplementary Fig. 1. This study used heterozygous transgenic mice harboring one targeted *Igh* allele, $iMyc^{E\mu}$, and one wild-type *Igh* allele. The targeted and wild-type *Igh* alleles were from strains 129SvJ (129) and C57BL/6 (B6), respectively. The genetic background of the $iMyc^{E\mu}$ colony was initially a variable, segregating mixture of 129 and B6 alleles. The mice used for the studies reported here were from generations three to six of an ongoing backcross of the $iMyc^{E\mu}$ transgene onto B6, resulting in an average content of B6 alleles from 93.8% (N_3) to 99.2% (N_6).

Turnover of "Premalignant" B Splenocytes. Cell surface marker expression was assessed using a FACSCalibur flow cytometer (BD Biosciences Pharmingen, San Diego, CA) and a panel of reagents useful for distinguishing subsets of hematopoietic cells. Total *Myc* mRNA levels, encoded by *Myc* and Myc^{His}, were determined in fluorescence-activated cell-sorting (FACS)-purified subpopulations of bone marrow B cells using the quantitative PCR assay on demand kit from Applied Biosystems (Foster City, CA). The turnover of MACS-purified $B220^+$ splenic B cells was measured by bromodeoxyuridine (BrdUrd) incorporation *in vivo* using the kit from BD Biosciences Pharmingen. For cell cycle analysis, B cells were stained with 50 μg/mL propidium iodide in buffer containing 0.1% sodium citrate and 0.1% Triton X-100 followed by FACS analysis. For determination of apoptosis, the FITC-conjugated monoclonal active caspase-3 antibody kit I was used (BD Bioscience). Proliferation of B cells *in vitro* was measured with the assistance of the colorimetric 3-(4,5-dimethylthiazol-2-yl)-5-(3-carboxymethoxyphenyl)-2-(4-sulfophenyl)-2*H*-tetrazolium, inner salt (MTS) assay (CellTiter 96 Aqueous Non-Radioactive Cell Proliferation Assay) from Promega (Madison, WI). To that end, $B220^+$ splenic cells were purified by MACS (Miltenyi, Auburn, CA) and grown for 48 hours in RPMI 1640 supplemented with 25 μg/mL lipopolysaccharide (LPS) from *Escherichia coli* 055:B5 (Sigma, St. Louis, MO), 10% fetal calf serum, 200 mmol/L L-glutamine, 50 μmol/L 2-mercaptoethanol, and penicillin/streptomycin (Life Technologies, Inc., Gaithersburg, MD). The immunologic competence of $iMyc^{E\mu}$ mice was assessed by s.c. injection of 100 μg of the synthetic peptide CLQLKEQKNAGTRTNEG that had been conjugated to keyhole limpet hemocyanin and emulsified in complete Freund's adjuvant. This was followed by two i.p. booster injections of keyhole limpet hemocyanin-peptide in incomplete Freund's adjuvant spaced 3 weeks apart. Total immunoglobulin levels and peptide-specific antibodies were measured by ELISA as previously described (16).

Histological and Immunohistochemical Examination of Tumors. Histological features of B-cell and plasma-cell tumors were assessed in 5-μm-thick sections of paraffin-embedded tissues stained with H&E, Giemsa according to Lennert, or periodic acid-Schiff. Apoptosis was determined by using the terminal deoxynucleotidyl transferase–mediated nick end labeling (TUNEL) assay (17). Briefly, tissue sections were digested with proteinase K and placed in a reaction buffer containing digoxigenin-labeled dUTP and deoxynucleotidyl transferase (15 units/μL). Sections were incubated with anti-digoxigenin antibody, developed with New Fuchsin substrate, and counterstained with hematoxylin. To measure proliferation of tumor cells *in vivo*, mice were pulsed with BrdUrd (200 mg/m^2 i.p., 8 hours), followed by immunostaining of tissue sections with antibody to BrdUrd. To visualize surface antigen expression in tumor cells, tissue sections were deparaffinized, treated with hot steam or microwaving to unmask antigen, incubated with 1% hydrogen peroxide to eliminate endogenous peroxidase activity, blocked with 5% goat serum, incubated with primary antibody overnight at 4°C, and detected by horseradish peroxidase–conjugated secondary antibody (1:200) and 3,3′-diaminobenzidine. Bcl-6 expression in diffuse large B-cell lymphomas was detected with a rabbit polyclonal antibody (N-3, Santa Cruz Biotechnology, Santa Cruz, CA) as previously described (18).

Molecular and Cytogenetic Studies with Lymphoblastic B-Cell Lymphoma. For Southern hybridization of clonotypic V(D)J rearrangements, genomic DNA obtained from tumor tissues was digested with *Eco*RI (for *Igh*) or *Eco*RI and *Bam*HI (for *Igk*), fractionated by electrophoresis on 0.7% agarose gels, transferred onto a nitrocellulose membrane, and hybridized to a [^{32}P]dCTP-labeled 1.5-kb *Hin*dIII/*Eco*RI *Igh* probe (pJ11) spanning J_H3 and Eμ or a 1.1-kb Cκ probe. The latter probe was generated by PCR using a primer pair (forward: 5′-GAT GCT GCA CCA ACT GTA TCC A; reverse: 5′-GGG GTG ATC AGC TCT CAG CTT) and method developed by Dr. Michael Kuehl (National Cancer Institute, NIH). For spectral karyotyping, metaphase chromosomes were prepared from primary tumor cells *ex vivo* or tumor cells cultured *in vitro* for 1.5 hours in 20 μg/mL Colcemid (Life Technologies). Cells were lysed in hypotonic KCl solution; chromosomes were fixed in methanol-acetic acid (3:1); and spectral

karyotyping analysis was done as previously described (19). For each tumor, at least 10 complete metaphase plates were analyzed.

Detection of *Myc*^{His} by Immunoblotting and Total *Myc* mRNA by Northern Blotting. Tissue samples were homogenized in 50 mmol/L TRIS, 150 mmol/L NaCl, 0.5% Triton X-100, 0.5% SDS, 0.5% sodium deoxycholate, and 10% glycerol. Proteins from clarified lysates (40 μg) were resolved electrophoretically in denaturing 10% SDS-PAGE gels and transferred by electroblotting to nitrocellulose membranes. Membranes were probed with rabbit anti-His_6-tag antibody (1:5,000, Clontech, Palo Alto, CA). The position of the *Myc*^{His} protein was visualized with horseradish peroxidase–conjugated goat anti-rabbit antibody (1:5,000; Amersham, Arlington Heights, IL) using the chemiluminescence detection kit from Amersham. To confirm equal loading, the membrane was stripped and reprobed using an antibody specific for -actin (Sigma). For Northern blot analysis of *Myc* mRNA, polyadenylated RNA was extracted from tumor nodules, fractionated by electrophoresis on formaldehyde-containing 1.0% agarose gels, transferred to Hybond N membranes, and hybridized to a *Myc* exon 1 probe (pMmyc54) that was nick translated to a specific activity of 2×10^8 cpm/μg (20).

Determination of *Myc* and *Myc*^{His} mRNA Levels by Allele-Specific Reverse Transcription–PCR. *Myc*^{His} and *Myc* expression was determined by semiquantitative reverse transcription–PCR (RT-PCR) using a common 5′ primer (5′-TCT CCA CTC ACC AGC ACA AC-3′) but 3′ primers specific either for *Myc*^{His} (5′-CCT CGA GTT AGG TCA GTT TA-3′) or wild-type *Myc* (5′-(5′-ATG GTG ATG GTG ATG ATG AC-3′). cDNA was synthesized using the AMV reverse transcriptase kit (Roche, Indianapolis, IN) and amplified by PCR using the following thermal cycling conditions: 95°C for 5 minutes (initial template denaturation) followed by 20 cycles of amplification at 62°C (primer annealing), 72°C (extension) and 95°C (melting), each for 1 minute. PCR amplification of the housekeeping gene *Gapd* (glyceraldehyde-3-phosphate dehydrogenase) was done for each sample as a control using the following primer pair: 5′-GGT GGA GCC AAA CGG GTC ATC ATC C-3′ and 5′-CAC ATT GGG GGT AGG AAC ACG GAA GG-3′.

Analysis of *Myc* Promoter Shift by RNase Protection Analysis. RNA was extracted from B220$^+$ MACS-purified splenic B cells and tumor tissues of iMyc^{Eμ} mice with the TRIZOL reagent (Invitrogen, San Diego, CA) and then treated with DNase I. RNA samples from mouse plasmacytomas TEPC 1165 and ABPC 20, pooled thymus glands from twenty 4- to 6-weeks-old BALB/c mice and splenic B cells from C57BL/6 mice were included as controls. A 1,144-base antisense RNA probe was synthesized by T7 RNA polymerase using a MAXIscript *in vitro* transcription kit from Ambion (Austin, TX). The probe was synthesized in the presence of [α-^{32}P]UTP at 800 Ci/mmol, 40 mCi/mL (PerkinElmer Life Sciences, New England Nuclear, Boston, MA) and purified on a 6% acrylamide-urea gel. The *Myc* probe covered sequences from an *Eco*RI star site 626 bp upstream of the P1 promoter to the *Sst*I site near the 3′ end of exon 1. Ribonuclease protection was done with the Ambion RPA III kit following the instructions of the manufacturer. Briefly, 10 μg of total RNA was hybridized with about 1 ng of *Myc* probe at 58°C for 16 hours, followed by digestion with 0.4 units of RNase A and 15 units of RNase T1 at 37°C for 30 minutes. The protected products were resolved on a 6% acrylamide-urea gel. Transcripts derived from the *Myc* P1 promoter protected 518 bases of the probe and transcripts derived from the P2 promoter protected 355 bases of the probe. Signals were quantitated with a Storm phosphor imager (Molecular Dynamics, Sunnyvale, CA) and normalized to correct signal strength for the number of uridine residues in the protected probe fragments. RNAs with known P1/P2 ratios of about 2 (TEPC 1165) and 0.4 (ABPC 20), respectively, were used as controls (21).

Detection of Point Mutations in Myc Amino-Terminal Transactivation Domain. Genomic DNA was purified from BLL using the Trizol reagent (Life Technologies), removing contaminating mRNA by digestion with Rnase A. *Myc*^{His} was amplified by PCR using the following thermal cycling conditions: 95°C for 5 minutes followed by 30 cycles of amplification at 62°C for 20 seconds, 72°C for 60 seconds, and 95°C for 20 seconds. PCR primer sequences were 5′-ACA ATC TGC GAG CCA GGA CAG GAC T-3′ (forward) and 5′-TCC TCA TCT TCT TGC TCT TCT TCA GAG T-3′ (reverse). The resultant amplicon was 942 bp long and contained the protein-encoding exons 2 and 3 of *Myc*^{His} together with the regulatory exon 1, which harbors the P1/P2 promoter. Normal *Myc* sequence was not amplified because the primers were separated by ~2.5 kb of intron 1 and 2 sequence, which was not present in the *Myc*^{His} cDNA. PCR products were sequenced using equipment and reagents from Applied Biosystems.

Immunoblotting of p19^{Arf}, Mdm2, and p53 and Detection of Deletions in *Ink4a* (p19^{ARF}). For immunoblotting, whole-cell protein extracts were prepared from primary tumors in ice-cold modified radioimmunoprecipitation assay buffer buffer [50 mmol/L Tris-HCl (pH 7.4), 1% NP40, 0.25% sodium deoxycholate, 150 mmol/L NaCl, 1 mmol/L EDTA, 1 mmol/L phenylmethylsulfonylfluoride, 1 μg/mL aprotinin, 1 μg/mL leupeptin, 1 μg/mL pepstatin, 1 mmol/L Na_3VO_4]. Undissolved material was sedimented in a microfuge (4°C, 7 minutes, 14,000 rpm) followed by measurement of protein in the supernatant. Protein (30 μg/lane) was separated on 10% SDS-PAGE gels, transferred to Protran nitrocellulose membranes (Schleicher & Schuell, Keene, NH), probed with antibody to mouse p19^{ARF} (Ab-80, Abcam, Cambridge, MA), p53 (FL-393, Santa Cruz), and Mdm2 (C-18, Santa Cruz) and detected by horseradish peroxidase–conjugated secondary antibody using the enhanced chemiluminescence kit from Amersham. For detection of deletions of exon 1 in the *Ink4a* locus, PCR was done. PCR-amplified indicator fragments of *Trp53* (p53) and *Myc* were included as controls. Genomic DNA was isolated from primary tumors using the Puregene DNA isolation kit (Gentra Systems, Minneapolis, MN) followed by amplification with the Expand High-Fidelity PCR kit (Roche). Thermal cycling conditions were as follows: denaturation at 94°C for 1 minute, primer annealing at 61°C for 30 seconds in case of *Ink4a* (p19^{ARF}) and *Myc*, or 58°C and 45 seconds in case of *Trp53*, followed by extension at 72°C for 45 seconds for the first 10 cycles and a progressive 5-second increase per cycle for the remaining 20 cycles. The following primer pairs were used: *Ink4a* (exon 1): 5′-ACT GAA TCT CCG CGA GGA AAG CGA ACT-3′ (forward) and 5′-GAA TCG GGG TAC GAC CGA AAG AGT-3′ (reverse), *Trp53* (exon 3) 5′-CTT TGA GGT TCG TGT TTG TGC CC-3′ (forward) and 5′-CCC TGA AGT CAT AAG ACA GCA AGG-3′ (reverse), and *Myc* (exon 2-3) 5′-GAC GAC GAG ACC TTC ATC AAG AAC-3′ (forward) and 5′-TCA CGC AGG GCA AAA AAG C-3′ (reverse).

Results

***Myc*^{His} Is Expressed throughout B-Cell Development.** Because onset and level of *Myc*^{His} expression during B-cell development are likely to play an important role in determining incidence and types of lymphomas that might arise in iMyc^{Eμ} mice, we assessed the expression of Myc^{His} protein in lysates of FACS-sorted B cells at different maturation stages using immunoblotting with antibody to the His_6 tag (Fig. 2*A*). B220$^+$CD43$^+$ pro-B cells (fraction ABC according to Hardy; refs. 22, 23) and B220$^+$CD43$^-$ pre-B cells (DEF) collected from the bone marrow exhibited a 1.7-fold difference in Myc^{His} levels after normalization to the actin loading controls (experiment 1). Further dissection of the pre-B cell compartment DEF into fractions D (early pre-B; B220$^+$CD43$^-$IgM$^-$) and EF (late pre-B; B220$^+$CD43$^-$IgM$^+$) showed that the Myc^{His} levels varied again in a similar range (~2-fold) in these fractions (experiment 2). Myc^{His} expression was also comparable in transitional and mature B splenocytes, including T1 B cells (IgM^{bright}IgD^{dull}), T2 B cells (IgM^{bright}IgD^{bright}), mature (M) B cells (IgM^{dull}IgD^{bright}), and sIg$^+$κ$^+$ B cells further separated based on CD138 expression (experiment 3). These results showed that *Myc*^{His} is overexpressed throughout B-cell development, presumably driven by the Eμ enhancer, which is thought to be active at relatively constant levels throughout B-cell development (24).

To determine the elevation of *Myc* mRNA caused by insertion of *Myc*^{His} in the vicinity of Eμ, we did quantitative PCR in three major B-cell fractions collected by FACS based on expression of B220 and IgM (Fig. 2*B*). Total *Myc* mRNA was ~10-fold higher in B220^{low}IgM$^-$ pro-B/pre-B cells (columns 1 and 4), B220^{low}IgM$^+$ transitional B cells (columns 2 and 5), and B220^{hi}IgM$^+$ mature

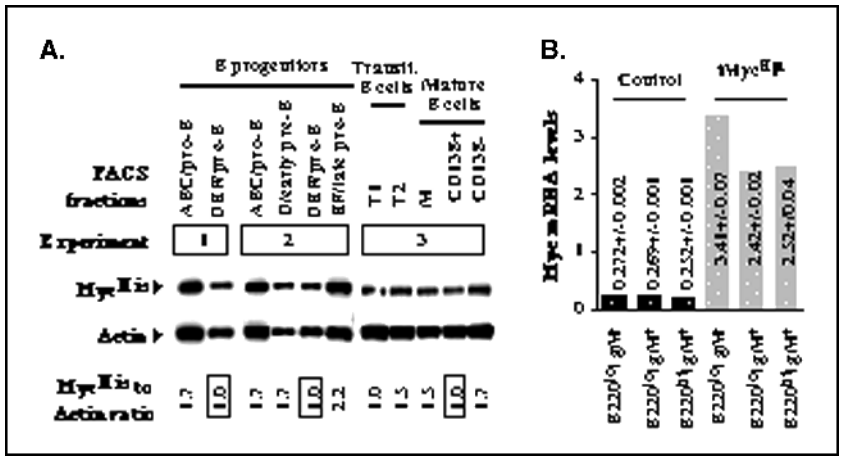

Figure 2. Overexpression of *Myc*^{His} throughout B-cell development in iMyc$^{E\mu}$ mice. *A,* expression of Myc^{His} at different stages of B-cell development. Samples with Myc^{His}/actin ratios set at 1.0 were used as internal standards in the three independent experiments. Myc^{His} expression is not strictly limited to B cells and is, therefore, leaky. This is shown in Supplementary Fig. 2, which shows transgene expression in splenic T cells, but not in splenic monocytes. *B,* elevated *Myc* mRNA expression in pro-B/pre-B cells (B220^{low}IgM^{-}), transitional B cells (B220^{low}IgM^{+}), and mature B cells (B220^{high}IgM^{+}) obtained from bone marrow of iMyc$^{E\mu}$ mice and nontransgenic littermates (*Control*). Average levels and SDs based on three independent measurements.

B cells (columns 3 and 6) obtained from the bone marrow of iMyc$^{E\mu}$ mice, compared with the same cell populations in normal littermates. These findings were consistent with Eμ controlling *Myc*^{His} expression and suggested that the constitutive overexpression of *Myc*^{His} leads to chronic changes in the B-cell compartment of iMyc$^{E\mu}$ mice before malignant transformation occurs.

Increased Turnover of Premalignant *Myc*^{His} Transgenic B cells *In vivo*. To evaluate whether constitutive expression of *Myc*^{His} leads to chronic activation and expansion of B cells before their malignant transformation, we studied proliferation and apoptosis in B cells from 4- to 6-months-old, tumor-free iMyc$^{E\mu}$ mice. FACS analysis of MACS-sorted B220^{+} splenocytes stained with propidium iodide showed that, on average, 4.73% *Myc*^{His} B cells were in S phase of the cell cycle, a 3.5-fold increase compared with B cells from nontransgenic littermates (1.36%; Fig. 3*A*). To better quantify the apparent increase in *Myc*^{His}-dependent proliferation, we labeled B cells with BrdUrd *in vivo* followed by FACS analysis. The *Myc*^{His}-transgenic B cells (8.79% BrdUrd^{+}) proliferated, on average, 3.8 times faster than controls (2.34% BrdUrd^{+}; Fig.3B). Increased proliferation of *Myc*^{His} B cells was accompanied by elevated apoptosis in these cells (7.46 ± 2.18%) compared with normal B cells (0.14 ± 0.02%), using reactivity for activated caspase 3 as the FACS label (Fig. 3*C*). The increased proliferation of *Myc*^{His} B cells *in vivo* noted above was also observed in cell culture upon examination of the LPS response using the MTS assay. MACS-purified B splenocytes from iMyc$^{E\mu}$ mice proliferated more vigorously than B cells from wild-type littermates after stimulation with three different doses of LPS (Fig. 3*D*).

We next evaluated whether *Myc*-transgenic B cells exhibit changes in surface marker expression compared with wild-type controls. FACS analysis using a panel of antibodies to B cell–associated differentiation and activation antigens showed that B cells from 4- to 6-months-old iMyc$^{E\mu}$ mice expressed heightened levels of costimulatory receptor CD40 (Fig. 4*A*, *top*) and activation markers CD38, CD86, and MHC class II (results not shown). In contrast, CD48 and CD95 (Fas) were down regulated (Fig. 4*A*, *center* and *bottom*). The down-regulation of Fas may be an adaptive change to counterbalance Myc-induced apoptosis (25), but this has not been shown here.

To assess whether the changes in the B-cell compartment of iMyc$^{E\mu}$ mice compromise immune responsiveness, we immunized the mice with the T cell–dependent antigen, CLQLKEQKNAGTRT-NEG-keyhole limpet hemocyanin. The response of transgenics and wild-type controls was indistinguishable, based on antigen-specific titers of IgM and the four IgG isotypes (Fig. 4*B*). Transgenic mice had also normal overall serum IgG and IgM levels compared with wild-type littermates, which served as controls (Fig. 4*C*). Stained sections of lymphoid tissues of 4- to 6-months-old mice revealed the long-term consequences of *Myc*^{His}-driven B-cell proliferation at the morphologic level. Spleen (Fig. 4*D*) and lymph nodes (not shown) of transgenic mice were enlarged relative to nontransgenic controls because of progressive, follicular hyperplasia indicative of B-cell accumulation *in vivo*. This finding indicated that in B cells of tumor-free iMyc$^{E\mu}$ mice, the balance of *Myc*-dependent proliferation and apoptosis is tipped in favor of proliferation, leading to characteristic prelymphomatous changes in these mice.

Development of Mature B-Cell and Plasma-Cell Neoplasms in iMyc$^{E\mu}$ Mice. To examine the possibility that *Myc*^{His}-dependent lymphomas might arise in iMyc$^{E\mu}$ mice, we monitored 109 mice for tumor development. The overall tumor incidence was 68% at 21 months of age (Fig. 5*A*). Histological examination of 76 tumor-bearing mice revealed three major tumor types (Fig. 5*B*), which appeared with similar latency. The most prevalent tumors were lymphoblastic B-cell lymphomas with a Burkitt-like "starry sky" morphology due to tingible body macrophages (ref. 26; Fig. 5*C*, *top*). Immunostaining showed that the tingible body macrophages engulfed TUNEL-positive cells (not shown). Lymphoblastic B-cell lymphomas were IgM^{+}IgD^{+}B220^{+}CD19^{+}CD5^{-} using flow cytometry and had a high proliferative index (>70%) after BrdUrd labeling *in vivo* (not shown). Nearly one quarter of the lymphomas were diagnosed as diffuse large B-cell lymphomas (26) strongly positive for Bcl-6 by immunohistochemistry (Fig. 5*C*, *center*). Another fifth of the lymphomas were CD19^{+}CD138^{+} plasmacytomas (Fig. 5*C*, *bottom*) that exhibited varying degrees of differentiation, including plasmablastic, anaplastic, and plasmacytic variants. Plasmacytoma produced monoclonal immunoglobulin of γ, α (shown in Fig. 5*C*, *bottom*), and μ isotypes. Although the morphologic characteristics of lymphoblastic B-cell lymphoma, diffuse large B-cell lymphoma, and plasmacytoma will be described in depth in a subsequent article, the findings presented here clearly indicated that *Myc*^{His} induced a spectrum of mature B-cell and plasma-cell tumors. Because lymphoblastic B-cell lymphoma was the most common lymphoma iMyc$^{E\mu}$ mice, it was chosen for further study described below.

Lymphoblastic B-Cell Lymphomas Are Monoclonal Tumors and Express *Myc*^{His} Predominantly from the P1 Promoter. Southern analysis of V(D)J recombination showed that lymphoblastic B-cell lymphomas had undergone clonotypic Igκ rearrangements

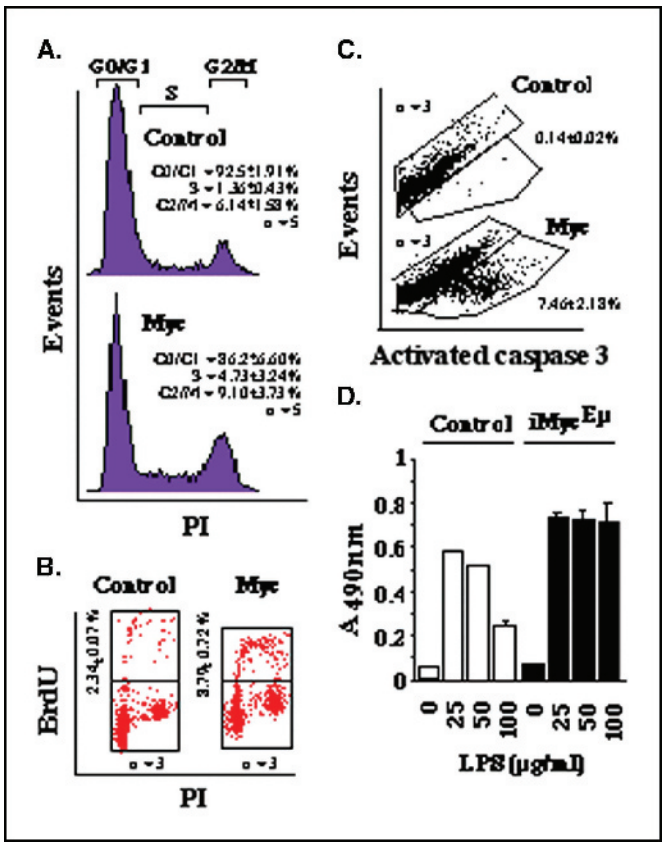

Figure 3. Increased turnover of premalignant B cells in tumor-free iMyc$^{E\mu}$ mice. *A,* FACS analysis indicates increased cell cycle progression in *Myc^{His}*-transgenic B cells (*bottom*) compared with normal B cells (*top*). Freshly isolated B220$^+$ splenocytes were stained with propidium iodide (*PI*) and cell cycle profiles determined by FACS. Means and SDs (%) of cells in three different cell cycle stages. The results are based on five independent determinations. *B,* increased proliferation in *Myc^{His}*-transgenic B cells (*right*) compared with normal B cells (*left*). B220$^+$ splenocytes were labeled with antibody to BrdUrd and analyzed by FACS to determine the fraction of dividing cells that had incorporated BrdUrd *in vivo* (*B*). Means and SDs (%) of BrdUrd$^+$ cells are shown. The results are based on three independent determinations. *C,* elevated apoptosis in *Myc^{His}*-transgenic B cells (*bottom*) relative to normal B cells (*top*). Splenic B cells were sorted using magnetic beads followed by labeling with antibody to activated caspase 3 and FACS analysis. The average FACS reactivity to activated caspase 3 was markedly increased in transgenic B cells (7.46%) compared with controls (0.14%) in three independent determinations. *D,* enhanced LPS response in iMyc$^{E\mu}$ B cells. MACS-purified B220$^+$ splenocytes from transgenic mice and nontransgenic littermates (*Control*) were cultured for 24 hours in the absence of LPS (*background control*) and presence of 25, 50, or 100 μg/mL LPS. Proliferation was measured using the MTS assay. Average results of three independent measurements.

(Fig. 6*A*, *left*). Rearrangements of *Igh* were also readily detected, but these were limited to the B6-derived locus (Fig. 6*A*, *right*). Western blotting with anti-His$_6$ antibody showed that lymphoblastic B-cell lymphoma invariably expressed Myc^{His}, although the expression levels varied (Fig. 6*B*, *left*). Myc^{His} protein was clearly elevated in lymphoblastic B-cell lymphoma compared with premalignant B splenocytes from iMyc$^{E\mu}$ mice and normal B splenocytes (negative controls) using immunocytochemistry (Figure 6*B*, *right*). Northern blotting showed that total *Myc* mRNA (*Myc^{His}* plus *Myc*) was overexpressed compared with controls (Fig. 6*C*). Estimation of the abundance of *Myc^{His}* and *Myc* mRNA by allele-specific RT-PCR showed that the bulk of the *Myc* message was encoded by the inserted transgene (Fig. 6*D*). A characteristic feature of *Myc* deregulation in human BL and mouse plasmacytoma is a shift in promoter usage from the second *Myc* promoter, P2, which initiates ~80% to 90% of *Myc* mRNA in normal B cells, to the first promoter, P1, which initiates ~10% to 20% of normal *Myc* mRNA. To evaluate whether mouse lymphoblastic B-cell lymphoma exhibited a shift in the primacy of promoter usage, RNase protection assays were done with primary lymphoblastic B-cell lymphoma. Two mouse plasmacytoma cell lines that displayed a pronounced promoter shift (TEPC 1165) or did not (ABPC 20) were included as positive and negative controls (21). The analysis (summarized in Fig. 7*A* and presented in detail in Supplementary Fig. 2) showed that lymphoblastic B-cell lymphoma exhibited the full P2 to P1 promoter shift in *Myc* expression. In contrast, B220$^+$ B cells from iMyc$^{E\mu}$ mice did not show a promoter shift relative to B220$^+$ B cells from normal B6 mice, BALB/c thymus, and ABPC 20. These findings suggested that the juxtaposition of *Myc* to Eμ is, on its own, not sufficient to cause the promoter shift. The shift seems to require additional changes associated with acquisition of the malignant phenotype of lymphoblastic B-cell lymphoma.

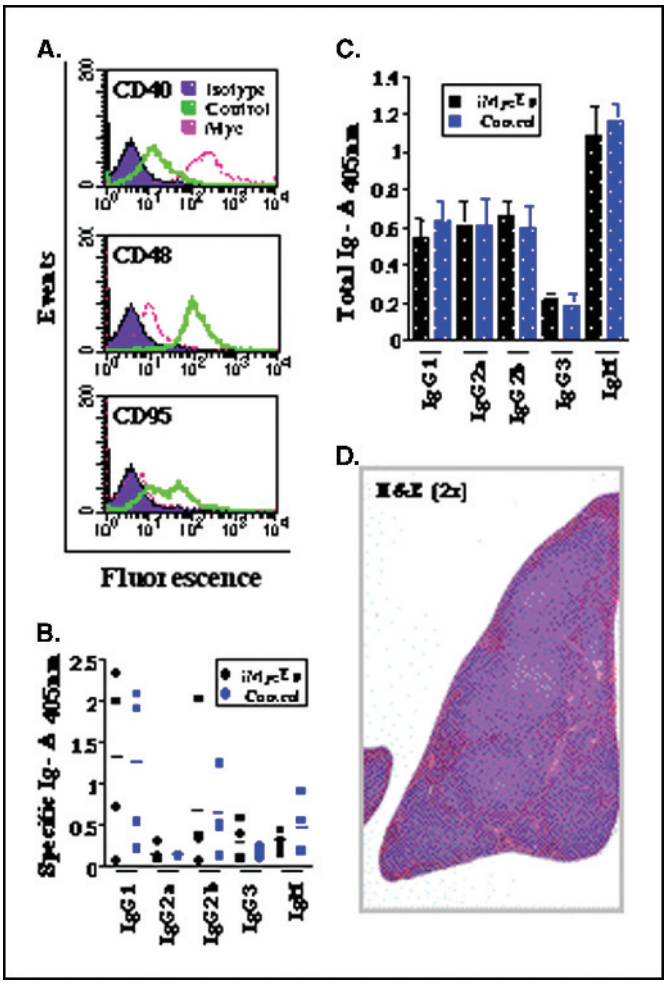

Figure 4. Lymphoid hyperplasia and normal immune response in tumor-free iMyc$^{E\mu}$ mice. *A,* up-regulation of CD40 and down-regulation of CD48 and CD95 (Fas) on the cell surface of premalignant B220$^+$ splenocytes obtained from iMyc$^{E\mu}$ transgenic mice (*pink*) and nontransgenic littermates (*green*). Shown are representative FACS histograms with isotype-specific antibody controls depicted in *purple*. *B* and *C,* normal immune response of iMyc$^{E\mu}$ mice after immunization with a thymus-dependent peptide antigen. Antigen-specific (*F*) and overall IgG and IgM titers (*G*) were determined by ELISA in transgenic mice and wild-type littermate controls. Means and SDs based on four mice in each group. *D,* lymphoid hyperplasia in the spleen of a 6-month-old tumor-free iMyc$^{E\mu}$ mouse. The enlarged white pulp (*blue*) occupies more than 90% of the tissue section stained with H&E.

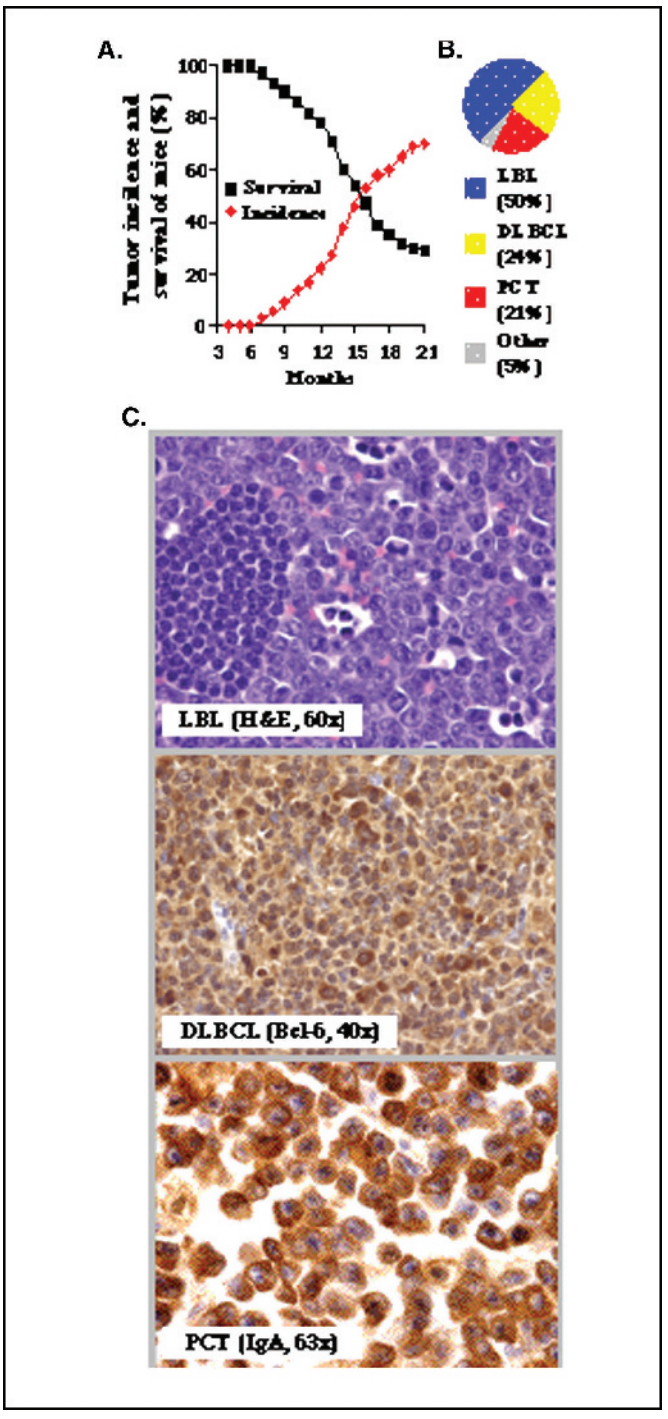

Figure 5. B-cell and plasma-cell tumors in iMyc$^{E\mu}$ mice. *A,* tumor incidence and survival of mice. *B,* graphical representation of the observed tumor spectrum: *LBL,* lymphoblastic B-cell lymphoma; *DLBCL,* diffuse large B-cell lymphoma; *PCT,* plasmacytoma. Tumor classification was difficult in 5% of cases, designated as *Other*. *C,* representative histologic tissue sections of the three main tumor types observed in the iMyc$^{E\mu}$ mice, either stained with H&E (*top*) or immunostained with antibody to Bcl-6 (*middle*) or IgA (*bottom*).

Point Mutations in *Myc* Transactivation Domain Are Rare in Lymphoblastic B-Cell Lymphoma. More than 60% of human BL and AIDS-associated B-cell lymphomas carrying *MYC*-activating chromosomal translocations harbor mutations in the rearranged *MYC* gene that alter the biological properties of the expressed MYC protein. The clustering of the great majority of these mutations in a highly conserved region of *MYC* amino-terminal transactivation domain (MYC homology box 1, MbI) suggests that these mutations were selected during tumor development. The underlying reason for this selection and the mechanism of mutagenesis in MbI are not known, but some circumstantial evidence points to VDJ hypermutation in germinal center B cells as the underlying mutagenic principle (27). To evaluate whether mouse lymphoblastic B-cell lymphomas contain point mutations in Myc^{His}, we sequenced the entire *Myc^{His}* gene (2.2 kb for both DNA strands) in 34 tumors obtained from 16 lymphoblastic B-cell lymphoma–bearing mice. 74.8 kb of DNA sequence analysis resulted in the detection of just one mutation, a tandem missense mutation, L56F/P57S, which was found in two tumors harvested from different anatomic sites in the same mouse (Fig. 7*B*). A recent tabulation of data from the literature (28) indicates that the P57S mutation is the second most common base substitution mutation in human BL, comprising 8 (14.5%) of 55 mutations in MbI. Interestingly, biological studies with the P57S allele have showed that this mutation results in lower oncogenic activity than wild-type *MYC* when assayed for neoplastic transformation of rat embryo cells in cooperation with the H-rasG12V oncogene (28). The significance of the L56F mutation, which has not been observed thus far in human BL, is not known. It may be an innocent "bystander" mutation in the present case of mouse lymphoblastic B-cell lymphoma.

Interruption of the Arf-Mdm-p53 Tumor Suppressor Axis in Lymphoblastic B-Cell Lymphoma. Myc-induced B-cell transformation and lymphomagenesis in Eμ-Myc transgenic mice (29) is limited by Myc-dependent apoptosis (30). One important mechanism of curtailing Myc-dependent apoptosis in Eμ-Myc mice is inactivation of the p19^{Arf}-Mdm2-p53 tumor suppressor pathway (31, 32). When activated, this pathway involves the up-regulation of p19^{Arf}, which results, in turn, in sequestration of Mdm2 and activation of the p53 checkpoint (33). To determine whether interruption of this pathway also plays a role in lymphoma development in the iMyc$^{E\mu}$ mice, we studied 26 lymphoblastic B-cell lymphomas using immunoblotting. Applying stringent assay conditions aimed at detecting pronounced alterations, we found changes in 12 (46.2%) of 26 tumors. Four (33%) of the 12 tumors with alterations overexpressed p19^{Arf} (Fig. 7*C*, LBL 1-4). Loss of p19^{Arf} protein expression, apparently due to biallelic deletions in the *Ink4a* locus, occurred in 6 (50%) of 12 tumors, as detected by Western blot and genomic PCR (LBL 5-10). Overexpression of Mdm2 was found in 2 tumors (17%, LBL 11-12). Elevation of (presumably dysfunctional) p53 was seen in 3 tumors (25%; LBL 2, 4, and 9, indicated by red squares), however, only in combination with overexpression of p19^{Arf} (LBL 2 and 4) or loss of p19^{Arf} (LBL 9). Irrespective of the underlying reasons, which may be complex, all of the above alterations are likely to result in the crippling of the p53 response (cell cycle arrest, apoptosis). Considering that loss of p53 (32, 34, 35) or p19^{Arf} (31, 32) accelerates Eμ-Myc-induced lymphoma development, our data suggest that the interruption of the p19^{Arf}-Mdm2-p53 pathway also plays a significant role in lymphomagenesis in iMyc$^{E\mu}$ mice (31).

Lymphoblastic B-Cell Lymphomas Contain Clonal Cytogenetic Alterations. Because Myc^{His}-dependent genomic instability (36) may be one mechanism by which the p53 pathway is interrupted during tumor progression, we used spectral karyotyping to analyze three randomly chosen lymphoblastic B-cell lymphomas. One of them exhibited a translocation/deletion at chromosome 11B (Fig. 8, *top*) and another one showed a large deletion in chromosome 13 (Fig. 8, *center*). The third tumor had

undergone tetraploidization and contained an extra copy of chromosome 18 (Fig. 8, *bottom*). Thus, three of three lymphoblastic B-cell lymphomas contained cytogenetic aberrations that were readily detectable by spectral karyotyping. Because these markers or extra chromosomes were found in 10 metaphase plates of each tumor, this provides additional evidence for the clonality of these tumors.

Discussion

Gene insertion was used to recreate as a germ line mutation in mice the *MYC/Myc*-activating *Igh* translocations seen in human endemic Burkitt lymphomas and certain mouse plasmacytomas. The newly developed mouse model, designated iMyc$^{E\mu}$, has several noteworthy features. First is the precise reconstruction of the translocation breakpoint region on human der(14) and mouse der(12), that is, the head-to-head juxtaposition of *Myc^{His}* and Eμ. Second is the potential for *Myc^{His}* to interact with the complete set of correctly spaced *Igh* enhancers, designed to create the same complex interplay of promoter and enhancer interactions that govern the expression of translocated *MYC/Myc* in human endemic Burkitt lymphoma/mouse plasmacytoma. Third is the insertion of *Myc^{His}* in the *Igh* chromatin domain, which presumably subjects the gene to the same higher-order regulatory influences (e.g., those imposed by chromatin remodeling and positional effects in the interphase nucleus) that affect *MYC/Myc* involved in the t(8;14)/T(12;15) exchange. Our finding that many of the heterozygous iMyc$^{E\mu}$ mice spontaneously developed lymphoblastic B-cell lymphoma, diffuse large B-cell lymphomas, and plasmacytomas suggests that the iMyc$^{E\mu}$ transgene reproduced the key features of the t(8;14)/T(12;15) translocation that initiate the development of endemic Burkitt lymphoma in humans and plasmacytoma in mice.

Our *Myc^{His}* transgene model of the endemic Burkitt lymphoma t(8;14)/plasmacytoma T(12;15) effectively induces B-cell neoplasia even though it differs from the "natural" chromosomal translocations found in the human and mouse tumors in at least three potentially important aspects. First, the natural translocations are spontaneously occurring somatic mutations in tumor precursors, whereas *Myc^{His}* is a germ line mutation present in all cells. Second, *Myc^{His}* insertion reproduced only the *MYC/Myc*-activating product of translocation, not the reciprocal product of translocation. Third, in endemic Burkitt lymphoma t(8;14), the breakpoints on chromosome 8 are scattered over a considerable genomic distance in the 5′ flank of *MYC* (37, 38), resulting in separation of *MYC* from Eμ by more than 340 kb (37) in some cases (class III translocations according to Cory 39). As shown here, these

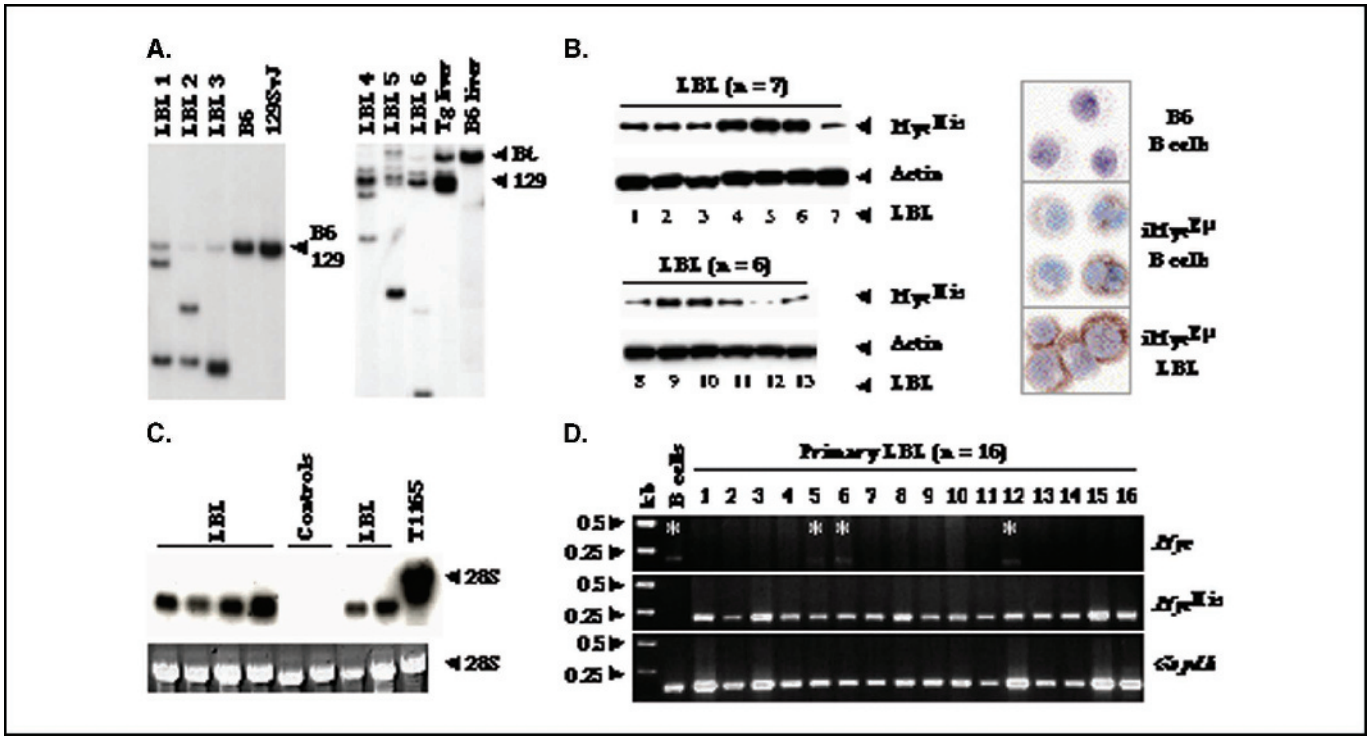

Figure 6. Lymphoblastic B-cell lymphomas are monoclonal tumors overexpressing *Myc^{His}*. *A,* clonotypic VDJ rearrangements. Shown are Southern blots that contain DNA from six tumors after *Eco*RI restriction digestion and hybridization to an Ig$_\kappa$ (*left*) or J$_H$ probe (*right*). Lymphoblastic B-cell lymphoma arose in mice that harbored one normal C57BL/6 (B6)-derived *Igh* allele and one mutant 129SvJ(129)-derived *Igh* allele with the *Myc^{His}*. The B6 allele is indicated by one fragment (6.3 kb), whereas the 129 allele is indicated by two fragments (5.3 and 5.1 kb) that are poorly separated on the gel. VDJ rearrangements occurred only on the B6 allele, indicated by a reduction of the fragment relative to the germ line fragment in iMyc$^{E\mu}$ liver (*Tg liver*) or liver from normal B6 mice. *B,* lymphoblastic B-cell lymphomas express Myc^{His} protein using Western blotting (*left*) and immunocytochemistry (*right*). *Left,* two immunoblots that contain lysates from 13 randomly chosen, primary lymphoblastic B-cell lymphomas. Myc^{His} was detected with an anti-His antibody. Anti-actin was used as loading control. *Right,* cytofuge specimens of lymphoblastic B-cell lymphoma cells (*bottom*) next to FACS-purified premalignant B cells from iMyc$^{E\mu}$ mice (*middle*), and normal splenic B cells from C57BL/6 mice (control, *top*) after immunostaining with an antibody to the histidine tag. *C,* lymphoblastic B-cell lymphomas overexpress *Myc* mRNA. Shown is a Northern blot that contains RNA samples from six primary lymphoblastic B-cell lymphoma. RNA samples obtained from two lymph nodes and the BALB/c plasmacytoma line, TEPC 1165, were included as negative and positive controls, respectively. The ethidium bromide–stained agarose gel showing the 28S rRNA band (*bottom*) is included as loading control. *D,* lymphoblastic B-cell lymphomas express *Myc* mRNA mainly from the inserted *Myc^{His}* gene. Shown are ethidium bromide–stained agarose gels with RT-PCR products that reflect the abundance of *Myc* mRNA (*top*), *Myc^{His}* mRNA (*middle*), and *Gapd* mRNA (*bottom*) in 16 primary lymphoblastic B-cell lymphomas and B220$^+$ C57BL/6 splenocytes (control sample). *White asterisks in the top,* presence of faint PCR indicator fragment. Size markers are in the *left-hand lane*.

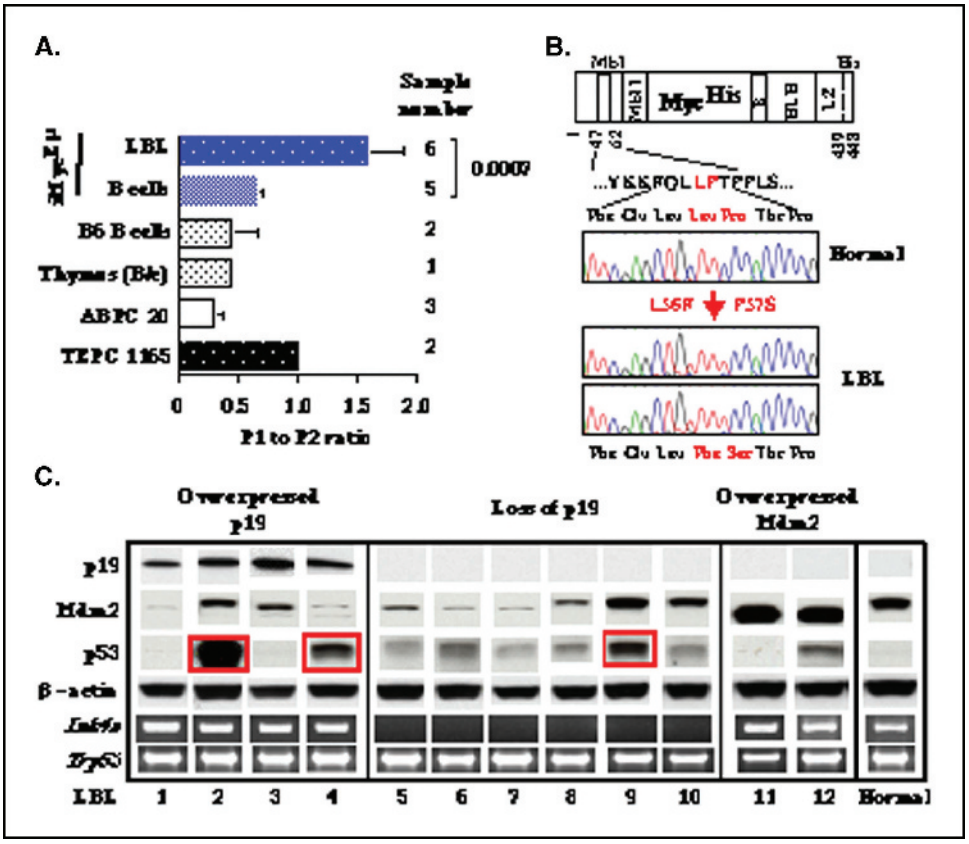

Figure 7. Lymphoblastic B-cell lymphomas exhibit the P2 to P1 promoter shift of *Myc* expression and distortions of the $p19^{Arf}$-Mdm2-p53 tumor suppressor axis. *A,* lymphoblastic B-cell lymphomas exhibit the P2 to P1 promoter shift of *Myc* expression. Summary of the experimental results presented in Supplementary Fig. 2. Mean values of normalized P1/P2 ratios and SDs of the mean are plotted. The normalization was based on the P1/P2 ratio in TEPC 1165, which was arbitrarily set at 1. The P1/P2 ratio was significantly elevated in lymphoblastic B-cell lymphoma relative to splenic B cells from iMyc mice (two-sided Student's *t* test; $P = 0.0007$). *B,* tandem point mutation in Myc homology box I, a primary lymphoblastic B-cell lymphoma. *Top,* scheme of the Myc^{His} protein that contains the two Myc homology boxes MbI and MbII, the basic region (*B*), the helix-loop-helix domain (*HLH*), the leucine zipper (*LZ*), and the histidine tag (*His*). The MbI domain spans residues 47 to 62. *Bottom,* histograms of DNA sequencing reactions of MbI nucleotides encoding residues 53 to 59 of normal *Myc* and mutated *Myc* found in two independent specimens in 1 of 16 primary lymphoblastic B-cell lymphomas. The mutated *Myc* gene harbored point mutations in two neighboring codons, resulting in L56F and P57S substitutions. *C,* $p19^{ARF}$, Mdm2, and p53 expression and biallelic *Ink4a* deletions in primary lymphoblastic B-cell lymphomas. Protein levels of $p19^{ARF}$, Mdm2 and p53 were compared by immunoblotting in 12 lymphomas (*LBL 1-12*) and B splenocytes from nontransgenic littermates (*Normal*), using β-actin as loading control. Two of three major isoforms of Mdm2 are discernable in some lanes (e.g., *LBL 3 and 4*). Potential deletions of the genes encoding $p19^{ARF}$ and p53 were assessed by genomic PCR for exon 1 of *Ink4a* and exon 2 of *Trp53*, respectively. Apparent biallelic deletions of *Ink4a* were found in LBL 5-10. Deletions of *Trp53* were not found.

aspects of endemic Burkitt lymphoma t(8;14)/plasmacytoma T(12;15) are not critical to the development of B-cell and plasma-cell neoplasms following *MYC/Myc*-activating translocation. It follows that the juxtaposition of *Myc* and Eμ in the appropriate chromosomal context of the *Igh* chromatin domain defines the minimal, critical feature of the endemic Burkitt lymphoma t(8;14)/plasmacytoma T(12;15) translocation. The long latency of B-cell and plasma-cell tumors developing in $iMyc^{Eμ}$ mice suggests that secondary oncogenic events complement Myc^{His} during lymphomagenesis. Alternatively, the oncogenic potential of Myc^{His} may be offset *in vivo* by factors that inhibit *Myc*-induced transformation (e.g., *Myc*-induced apoptosis). The apparent occurrence of t(8;14)(q24;q32) in healthy blood donors (40), the repeated detection of T(12;15) in normal mice (41–43), and recent insights from mouse models of nonhematopoietic cancer driven by inducible *Myc* transgenes (44, 45) support this view.

The occurrence of plasmacytoma in ~20% of the tumor-bearing $iMyc^{Eμ}$ mice suggests that B cells bearing our model of *Myc*-activating translocation sometimes acquire the same subsequent genetic alterations that lead to the development of plasmacytoma following somatic acquisition of T(12;15). Plasmacytoma have not been observed in the Eμ-MYC/Myc and YAC-MYC mice. What mechanisms might be responsible for the unique property of the $iMyc^{Eμ}$ transgene to induce plasma cell tumors? One feature that distinguishes the $iMyc^{Eμ}$ mice from the Eμ-MYC/Myc and YAC-MYC mice is the genomic integration site of the *Myc* transgene. Whereas this site is ectopic in the Eμ-Myc and YAC-MYC, the insertion site of the Myc^{His} transgene in $iMyc^{Eμ}$ corresponds precisely to the t(8;14)/T(12;15) translocation break site in endemic Burkitt lymphoma/T(12;15). The strategic location of Myc^{His} in *Igh* may link timing and level of *Myc* activation to the developmentally controlled accessibility (46) and activity (47) of the *Igh* chromatin domain (48), generating thereby a temporal and quantitative pattern of Myc^{His} activation that is conducive to plasma cell tumors. A second distinguishing feature of the $iMyc^{Eμ}$ is the potential for Myc^{His} to interact with Eα and Eδ in addition to Eμ. The crucial importance of the *Myc*-Eα interaction for *Myc* deregulation in plasma cell tumors has been clearly shown (12). The *in vivo* relevance of the *Myc*-Eδ interaction has been recently noted by the surprising observation that Eμ is dispensable for *MYC* expression and lymphomagenesis in the YAC-MYC mouse (11), in which Eμ can apparently be substituted for by the Eδ enhancer (49).

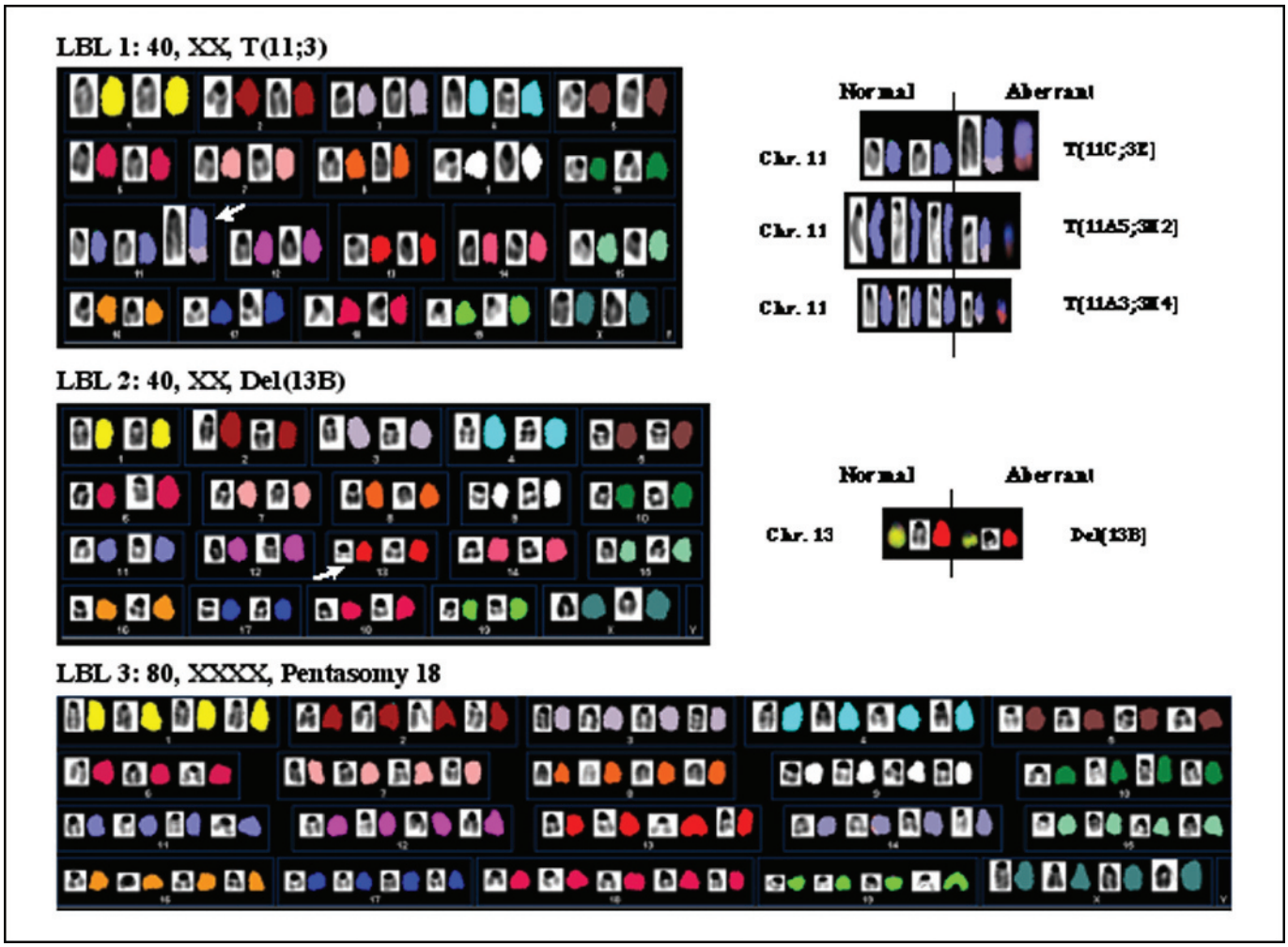

Figure 8. Chromosomal aberrations in lymphoblastic B-cell lymphoma detected by spectral karyotyping. Shown are a nonreciprocal T(11;3) translocation and a large internal deletion of chromosome 13B found in two primary tumors. Aberrant chromosomes are depicted in spectral karyotyping display colors (*middle*) and classification colors (*right*) next to inverted 4′,6-diamidino-2-phenylindole images (*left*). Normal chromosomes (*Chr.*) 11 and 13 are included for comparison. The T(11;3) was highly variable in different metaphases, presumably reflecting ongoing genomic instability of the chromosome. Three variants of T(11;3) from different metaphase spreads of LBL 1 are depicted to the right of the complete spectral karyotyping karyotype of this tumor. An image of Del 13B found in LBL 2 is also shown.

Thus, the ability of the iMyc$^{E\mu}$ to promote plasma cell transformations may be created by the complex interplay of *Myc*^{His} with all three *Igh* enhancers taking place in the appropriate genomic context of the *Igh* domain.

The iMyc$^{E\mu}$ mice were generated as part of a program to recreate and study in transgenic mice the molecular and oncogenic consequences of *MYC/Myc*-activating t(8;14)/T(12;15) translocations that characterize human and mouse B-cell and plasma-cell tumors, such as human endemic Burkitt lymphoma and mouse plasmacytoma. Among the new opportunities afforded by the iMyc$^{E\mu}$ is the identification of the secondary oncogenic events that complement *Myc* during neoplastic transformation, leading to lymphoblastic B-cell lymphoma in most cases, but diffuse large B-cell lymphomas and plasmacytoma in the others. Furthermore, although strain iMyc$^{E\mu}$ was not developed to model human endemic Burkitt lymphoma or any other specific type of human NHL in mice, it may provide guidance for possible future attempts to model human BL in mice more accurately. Human BL exhibits the phenotype of a germinal center (GC) B cell and contains somatic mutations in expressed immunoglobulin variable and *MYC* genes, indicating that the tumors have germinal center experience (50). Human BL acquire *MYC* translocations as spontaneous somatic mutations that are thought to be accidents of VDJ hypermutation (endemic Burkitt lymphoma) and isotype switching (sBL/iBL) in the germinal center (51). Human BL contains clonal EBV (52) and expresses the EBV-encoded EBNA-1 protein (53), which is consistent with malignant transformation occurring in an EBV-infected centroblast differentiating into a memory B cell (54). These features of human BL suggest that in order to model this neoplasm in mice more precisely, *Myc* activation should be delayed to the germinal center stage, for example, by placing *Myc* under control of a germinal center-specific promoter. *Myc* transgenes of this sort should then be combined with EBNA-1 transgenes (55) that could perhaps also be improved by targeting expression to germinal center B cells. Although these approaches may help to settle the long-standing thorny question of whether EBV plays an active role in the development of BL or is just a passive passenger in the tumor cells (56), the present study has shown that the iMyc$^{E\mu}$ transgene is a valuable model of endemic Burkitt lymphoma t(8;14) that predictably induces B-cell and plasma-cell tumors in mice.

Acknowledgments

Received 1/27/2004; revised 12/6/2004; accepted 12/13/2004.

The costs of publication of this article were defrayed in part by the payment of page charges. This article must therefore be hereby marked advertisement in accordance with 18 U.S.C. Section 1734 solely to indicate this fact.

We thank the following (from the National Cancer Institute): Lisa Craig, Tina Wellington, Nicole Wrice, and Wendy DuBois for genotyping and assistance with the mouse experiments; Eileen Southon for expert help with gene targeting; Elizabeth Mushinski for immunohistochemistry; Drs. Alexander L. Kovalchuk for generating the tumor incidence and survival curve; W. Michael Kuehl for the Igκ probe, reading an earlier version of the manuscript, and making helpful suggestions; Michael Potter for stimulating scientific discussion; and Beverly Mock for support; Drs. Hua Gu for the genomic clone (IgM DQ52) and Chen Feng Qi for Bcl-6 detection (both from the National Institute of Allergy and Infectious Diseases); and Dr. Georgina F. Miller (Veterinary Resources Program, NIH) for expert advice on tumor classification.

References

1. Dalla-Favera R, Bregni M, Erikson J, et al. Human c-*myc* onc gene is located on the region of chromosome 8 that is translocated in Burkitt lymphoma cells. Proc Natl Acad Sci U S A 1982;79:7824–7.
2. Taub R, Kirsch I, Morton C, et al. Translocation of the c-*myc* gene into the immunoglobulin heavy chain locus in human Burkitt lymphoma and murine plasmacytoma cells. Proc Natl Acad Sci U S A 1982;79:7837–41.
3. Janz S, Müller J, Shaughnessy J, Potter M. Detection of recombinations between c-*myc* and immunoglobulin switch α in murine plasma cell tumors and preneoplastic lesions by polymerase chain reaction. Proc Natl Acad Sci U S A 1993;90:7361–5.
4. Kovalchuk AL, Kim JS, Park SS, et al. IL-6 transgenic mouse model for extraosseous plasmacytoma. Proc Natl Acad Sci U S A 2002;99:1509–14.
5. Boxer LM, Dang CV. Translocations involving c-*myc* and c-*myc* function. Oncogene 2001;20:5595–610.
6. Adams JM, Harris AW, Pinkert CA, et al. The c-*myc* oncogene driven by immunoglobulin enhancers induces lymphoid malignancy in transgenic mice. Nature 1985; 318:533–8.
7. Suda Y, Aizawa S, Hirai S, et al. Driven by the same Ig enhancer and SV40 T promoter ras induced lung adenomatous tumors, myc induced pre-B cell lymphomas and SV40 large T gene a variety of tumors in transgenic mice. EMBO J 1987;6:4055–65.
8. Schmidt EV, Pattengale PK, Weir L, Leder P. Transgenic mice bearing the human c-*myc* gene activated by an immunoglobulin enhancer: a pre-B-cell lymphoma model. Proc Natl Acad Sci U S A 1988;85:6047–51.
9. Yukawa K, Kikutani H, Inomoto T, et al. Strain dependency of B and T lymphoma development in immunoglobulin heavy chain enhancer (E mu)-myc transgenic mice. J Exp Med 1989;170:711–26.
10. Butzler C, Zou X, Popov AV, Bruggemann M. Rapid induction of B-cell lymphomas in mice carrying a human IgH/c-*myc* YAC. Oncogene 1997;14:1383–8.
11. Palomo C, Zou X, Nicholson IC, Butzler C, Bruggemann M. B-cell tumorigenesis in mice carrying a yeast artificial chromosome-based immunoglobulin heavy/c-*myc* translocus is independent of the heavy chain intron enhancer (Emu). Cancer Res 1999;59: 5625–8.
12. Madisen L, Groudine M. Identification of a locus control region in the immunoglobulin heavy-chain locus that deregulates c-*myc* expression in plasmacytoma and Burkitt's lymphoma cells. Genes Dev 1994;8: 2212–26.
13. Thomas KR, Capecchi MR. Site-directed mutagenesis by gene targeting in mouse embryo-derived stem cells. Cell 1987;51:503–12.
14. Gu H, Zou YR, Rajewsky K. Independent control of immunoglobulin switch recombination at individual switch regions evidenced through Cre-loxP-mediated gene targeting. Cell 1993;73:1155–64.
15. Langa F, Lafon I, Vandormael-Pournin S, et al. Healthy mice with an altered c-*myc* gene: role of the 3′ untranslated region revisited. Oncogene 2001;20: 4344–53.
16. Weng QP, Kozlowski M, Belham C, et al. Regulation of the p70 S6 kinase by phosphorylation *in vivo*. Analysis using site-specific anti-phosphopeptide antibodies. J Biol Chem 1998;273:16621–9.
17. Gavrieli Y, Sherman Y, Ben-Sasson SA. Identification of programmed cell death *in situ* via specific labeling of nuclear DNA fragmentation. J Cell Biol 1992;119: 493–501.
18. Qi CF, Hori M, Coleman AE, et al. Genomic organisation and expression of BCL6 in murine B-cell lymphomas. Leuk Res 2000;24:719–32.
19. Liyanage M, Coleman A, du Manoir S, et al. Multicolour spectral karyotyping of mouse chromosomes. Nat Genet 1996;14:312–5.
20. Bauer SR, Piechaczyk M, Nordan RP, et al. Altered myc gene transcription and intron-induced stabilization of myc RNAs in two mouse plasmacytomas. Oncogene 1989;4:615–23.
21. Yang JQ, Bauer SR, Mushinski JF, Marcu KB. Chromosome translocations clustered 5′ of the murine c-*myc* gene qualitatively affect promoter usage: implications for the site of normal c-*myc* regulation. EMBO J 1985;4:1441–7.
22. Hardy RR, Carmack CE, Shinton SA, Kemp JD, Hayakawa K. Resolution and characterization of pro-B and pre-pro-B cell stages in normal mouse bone marrow. J Exp Med 1991;173:1213–25.
23. Hardy RR, Li YS, Allman D, et al. B-cell commitment, development and selection. Immunol Rev 2000; 175:23–32.
24. Ong J, Stevens S, Roeder RG, Eckhardt LA. 3′ IgH enhancer elements shift synergistic interactions during B cell development. J Immunol 1998;160:4896–903.
25. Hueber AO, Zornig M, Lyon D, et al. Requirement for the CD95 receptor-ligand pathway in c-*Myc*-induced apoptosis [see comments]. Science 1997;278:1305–9.
26. Morse HC III, Anver MR, Fredrickson TN, et al. Bethesda proposals for classification of lymphoid neoplasms in mice. Blood 2002;100:246–58.
27. Pasqualucci L, Neumeister P, Goossens T, et al. Hypermutation of multiple proto-oncogenes in B-cell diffuse large-cell lymphomas. Nature 2001;412:341–6.
28. Chang DW, Claassen GF, Hann SR, Cole MD. The c-*Myc* transactivation domain is a direct modulator of apoptotic versus proliferative signals. Mol Cell 2000;20:4309–19.
29. Cory S, Adams JM. The Bcl2 family: regulators of the cellular life-or-death switch. Nat Rev Cancer 2002;2: 647–56.
30. Zhou P, Levy NB, Xie H, et al. MCL1 transgenic mice exhibit a high incidence of B-cell lymphoma manifested as a spectrum of histologic subtypes. Blood 2001;97: 3902–9.
31. Eischen CM, Weber JD, Roussel MF, Sherr CJ, Cleveland JL. Disruption of the ARF-Mdm2-p53 tumor suppressor pathway in Myc-induced lymphomagenesis. Genes Dev 1999;13:2658–69.
32. Schmitt CA, McCurrach ME, de Stanchina E, Wallace-Brodeur RR, Lowe SW. INK4a/ARF mutations accelerate lymphomagenesis and promote chemoresistance by disabling p53. Genes Dev 1999;13:2670–7.
33. Sherr CJ. The INK4a/ARF network in tumour suppression. Nat Rev Mol Cell Biol 2001;2:731–7.
34. Cory S, Vaux DL, Strasser A, Harris AW, Adams JM. Insights from Bcl-2 and Myc: malignancy involves abrogation of apoptosis as well as sustained proliferation. Cancer Res 1999;59:1685–92s.
35. Hsu B, Marin MC, el-Naggar AK, et al. Evidence that c-*myc* mediated apoptosis does not require wild-type p53 during lymphomagenesis. Oncogene 1995;11:175–9.
36. Mai S, Mushinski JF. c-*Myc*-induced genomic instability. J Environ Pathol Toxicol Oncol 2003;22: 179–99.
37. Joos S, Falk MH, Lichter P, et al. Variable breakpoints in Burkitt lymphoma cells with chromosomal t(8;14) translocation separate c-*myc* and the IgH locus up to several hundred kb. Hum Mol Genet 1992;1: 625–32.
38. Shiramizu B, Barriga F, Neequaye J, et al. Patterns of chromosomal breakpoint locations in Burkitt's lymphoma: relevance to geography and Epstein-Barr virus association. Blood 1991;77:1516–26.
39. Cory S. Activation of cellular oncogenes in hemopoietic cells by chromosome translocation. Adv Cancer Res 1986;47:189–234.
40. Müller JR, Janz S, Goedert JJ, Potter M, Rabkin CS. Persistence of immunoglobulin heavy chain/c-*myc* recombination-positive lymphocyte clones in the blood of human immunodeficiency virus-infected homosexual men. Proc Natl Acad Sci U S A 1995;92:6577–81.
41. Müller JR, Jones GM, Potter M, Janz S. Detection of immunoglobulin/c-*myc* recombinations in mice that are resistant to plasmacytoma induction. Cancer Res 1996;56:419–23.
42. Müller JR, Jones GM, Janz S, Potter M. Migration of cells with immunoglobulin/c-*myc* recombinations in lymphoid tissues of mice. Blood 1997;89:291–6.
43. Roschke V, Kopantzev E, Dertzbaugh M, Rudikoff S. Chromosomal translocations deregulating c-*myc* are associated with normal immune responses. Oncogene 1997;14:3011–6.
44. Pelengaris S, Khan M, Evan GI. Suppression of Myc-induced apoptosis in β cells exposes multiple oncogenic properties of Myc and triggers carcinogenic progression. Cell 2002;109:321–34.
45. Pelengaris S, Khan M, Evan G. c-MYC: more than just a matter of life and death. Nat Rev Cancer 2002;2:764–76.
46. Chowdhury D, Sen R. Stepwise activation of the immunoglobulin mu heavy chain gene locus. EMBO J 2001;20:6394–403.
47. Shi X, Eckhardt LA. Deletional analyses reveal an essential role for the hs3b/hs4 IgH 3′ enhancer pair in an Ig-secreting but not an earlier-stage B cell line. Int Immunol 2001;13:1003–12.
48. Ratsch A, Joos S, Kioschis P, Lichter P. Topological organization of the MYC/IGK locus in Burkitt's lymphoma cells assessed by nuclear halo preparations. Exp Cell Res 2002;273:12–20.
49. Mundt CA, Nicholson IC, Zou X, et al. Novel control motif cluster in the IgH δ-γ 3 interval exhibits B cell-specific enhancer function in early development. J Immunol 2001;166:3315–23.
50. Chapman CJ, Wright D, Stevenson FK. Insight into Burkitt's lymphoma from immunoglobulin variable region gene analysis. Leuk Lymphoma 1998;30:257–67.
51. Kuppers R, Dalla-Favera R. Mechanisms of chromosomal translocations in B cell lymphomas. Oncogene 2001;20:5580–94.
52. Thorley-Lawson DA, Gross A. Persistence of the Epstein-Barr virus and the origins of associated lymphomas. N Engl J Med 2004;350:1328–37.
53. Gulley ML, Raphael M, Lutz CT, Ross DW, Raab-Traub N. Epstein-Barr virus integration in human lymphomas and lymphoid cell lines. Cancer 1992;70:185–91.
54. Kelly G, Bell A, Rickinson A. Epstein-Barr virus-associated Burkitt lymphomagenesis selects for down-regulation of the nuclear antigen EBNA2. Nat Med 2002;8:1098–104.
55. Drotar ME, Silva S, Barone E, et al. Epstein-Barr virus nuclear antigen-1 and Myc cooperate in lymphomagenesis. Int J Cancer 2003;106:388–95.
56. Polack A, Hortnagel K, Pajic A, et al. c-*myc* activation renders proliferation of Epstein-Barr virus (EBV)-transformed cells independent of EBV nuclear antigen 2 and latent membrane protein 1. Proc Natl Acad Sci U S A 1996;93:10411–6.